ACS APPLIED MATERIALS & INTERFACES

Research Article

www.acsami.org

Flexible Hybrid Membranes with $Ni(OH)_2$ Nanoplatelets Vertically Grown on Electrospun Carbon Nanofibers for High-Performance Supercapacitors

Longsheng Zhang,[†] Qianwei Ding,[†] Yunpeng Huang,[†] Huahao Gu,[†] Yue-E Miao,[*,‡] and Tianxi Liu[*,†,‡]

[†]State Key Laboratory of Molecular Engineering of Polymers, Department of Macromolecular Science, Fudan University, 220 Handan Road, Shanghai 200433, P. R. China

[‡]State Key Laboratory of Modification of Chemical Fibers and Polymer Materials, College of Materials Science and Engineering, Donghua University, 2999 North Renmin Road, Shanghai 201620, P. R. China

Supporting Information

ABSTRACT: The practical applications of transition metal oxides and hydroxides for supercapacitors are restricted by their intrinsic poor conductivity, large volumetric expansion, and rapid capacitance fading upon cycling, which can be solved by optimizing these materials to nanostructures and confining them within conductive carbonaceous frameworks. In this work, flexible hybrid membranes with ultrathin $Ni(OH)_2$ nanoplatelets vertically and uniformly anchored on the electrospun carbon nanofibers (CNF) have been facilely prepared as electrode materials for supercapacitors. The $Ni(OH)_2$/CNF hybrid membranes with three-dimensional macroporous architectures as well as hierarchical nanostructures can provide open and continuous channels for rapid diffusion of electrolyte to access the electrochemically active $Ni(OH)_2$ nanoplatelets. Moreover, the carbon nanofiber can act both as a conductive core to provide efficient transport of electrons for fast Faradaic redox reactions of the $Ni(OH)_2$ sheath, and as a buffering matrix to mitigate the local volumetric expansion/contraction upon long-term cycling. As a consequence, the optimized $Ni(OH)_2$/CNF hybrid membrane exhibits a high specific capacitance of 2523 F g^{-1} (based on the mass of $Ni(OH)_2$, that is 701 F g^{-1} based on the total mass) at a scan rate of 5 mV s^{-1}. The $Ni(OH)_2$/CNF hybrid membranes with high mechanical flexibility, superior electrical conductivity, and remarkably improved electrochemical capacitance are condsidered as promising flexible electrode materials for high-performance supercapacitors.

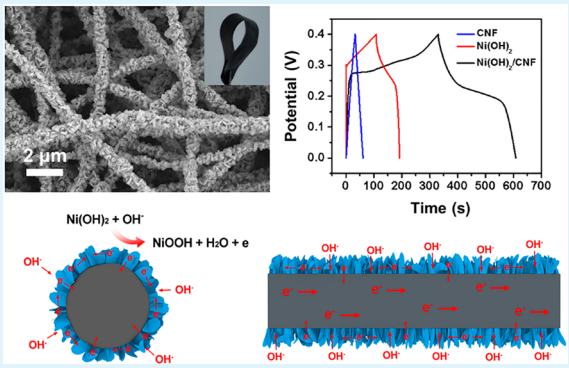

KEYWORDS: *electrospinning, $Ni(OH)_2$, carbon nanofibers, membranes, supercapacitors*

1. INTRODUCTION

The ever-increasing demand for efficient energy storage has accelerated the development of advanced energy storage and conversion systems, such as lithium-ion batteries, supercapacitors, solar cells, and fuel cells.[1−5] Among them, supercapacitors have become one of the main power sources for applications in portable electronic devices, owing to high power density, fast charging/discharging rate, long cycle life, and environmental benignity.[6−9] Recently, the great interest in portable and flexible electronics has created a strong driving force for the development of flexible energy storage devices with high capacitive performance. In order to fulfill this demand, it is urgently needed to explore efficient assembly approaches for the fabrication of flexible electrodes with robust mechanical property and excellent electrochemical performance.[10]

Generally, traditional carbon-based electrochemical double-layer capacitors (EDLCs) are based on physical adsorption/desorption of ions on the surface of an electrode, usually resulting in low capacitance and energy density.[11−14] To address this issue, one feasible and effective approach is to optimize the pseudocapacitive materials to nanostructures and confine them within a conductive carbonaceous matrix.[15−17] Recently, transition metal oxides and hydroxides (e.g., NiO, RuO_2, MnO_2, $Ni(OH)_2$, etc.) have been widely explored as excellent electrode materials for pseudocapacitors due to their high theoretical specific capacitances and fast multielectron surface Faradaic redox reactions.[18−21] In particular, $Ni(OH)_2$ has a high theoretical specific capacitance (2082 F g^{-1}) as well as many excellent properties, including being an abundant resource and having low cost, environmental friendliness, well-defined redox behavior, and high redox activity. However, the practical applications of $Ni(OH)_2$ materials are severely hindered by their poor conductivity, large volumetric

Received: August 14, 2015
Accepted: September 21, 2015
Published: September 21, 2015

DOI: 10.1021/acsami.5b07528
ACS Appl. Mater. Interfaces 2015, 7, 22669−22677

expansion, rapid capacity fading, and inferior electrochemical efficiency during the long-term Faradaic redox reactions.[22] For this reason, hybrid electrode materials with synergistically enhanced electrochemical performance can be achieved through confining $Ni(OH)_2$ materials within conductive carbon-based frameworks to construct hybrid nanostructures.[23,24]

Among various kinds of carbon materials, electrospun carbon nanofibers (CNFs) have attracted tremendous attention, owing to their large specific surface area, high mechanical flexibility, and low cost. Notably, electrospinning is a straightforward and efficient technique for fabricating self-standing nanofiber membranes with a unique three-dimensional (3D) fiber network, good structural stability, and high flexibility. Within the membrane, the nanofibers are able to interconnect with each other and form a 3D macroporous architecture, which can provide a high-surface-area template for further growth of electrochemically active pseudocapacitive materials to construct hierarchical nanocomposites.[25−27] Moreover, the carbon nanofiber can act both as a conductive core to provide efficient transport of electrons across the interfaces for fast Faradaic redox reactions of the pseudocapacitive materials, and as a buffering matrix to accommodate their local volumetric expansion/contraction upon long-term cycling. It is reported that many polymers, including poly(vinylidene fluoride), polyacrylonitrile, polystyrene, and poly(vinyl alcohol), have been employed as precursors to prepare carbon nanofibers via the combination of electrospinning and subsequent carbonization. However, their disadvantages, such as poor mechanical strength, inferior thermal stability, and low electrical conductivity, cannot fulfill the demand for flexible electrodes with excellent mechanical property and electrochemical performance.[28] On the other hand, polyimide (PI), as one kind of high-performance engineering polymers, has attracted extensive attention due to its excellent thermal stability and outstanding mechanical properties.[29] Besides, PI-based carbon nanofibers possess high electrical conductivity.[30] Therefore, it is expected to be an efficient approach to fabricate flexible electrodes by employing electrospun PI-based CNF membranes as self-standing and conductive substrates for high-performance energy storage devices.

Herein, we demonstrate a facile and scalable process to fabricate flexible $Ni(OH)_2$/CNF hybrid membranes as electrode materials for supercapacitors through the combination of electrospinning and chemical bath deposition (CBD). By utilizing electrospun PI-based CNF membrane as template, hierarchical nanostructures are nicely constructed with ultrathin $Ni(OH)_2$ nanoplatelets vertically anchored on the carbon nanofibers, which can effectively prevent the agglomeration of $Ni(OH)_2$ and mitigate their volumetric expansion during the repetitive cycling process. Additionally, the conductive carbon nanofiber core can provide efficient transport of electrons for fast Faradaic redox reactions of the electrochemically active $Ni(OH)_2$ sheath. Moreover, the 3D macroporous architecture derived from the interconnected nanofiber networks can significantly increase the porosity and provide continuous ion-transportation channels, thus facilitating the rapid diffusion of electrolyte to access the active sites of $Ni(OH)_2$ nanoplatelets. Besides, in this work, the influences of the reaction time and precursor concentration of $Ni(NO_3)_2$ during the CBD process have been investigated in detail. The results reveal that the optimized $Ni(OH)_2$/CNF hybrid membrane obtained with the reaction time of 6 h and the $Ni(NO_3)_2$ concentration of 0.025 M exhibits the highest specific capacitance of 2523 F g^{-1} (based on the mass of $Ni(OH)_2$, that is 701 F g^{-1} based on the total mass) at a scan rate of 5 mV s^{-1}, which is much superior to either neat CNF membrane or pure $Ni(OH)_2$ powder, confirming the great potential of $Ni(OH)_2$/CNF hybrid membranes as high-performance electrode materials for supercapacitors.

2. EXPERIMENTAL SECTION

2.1. Materials. Pyromellitic dianhydride (PMDA), 4,4′-oxidianiline (ODA), nickel(II) nitrate hexahydrate ($Ni(NO_3)_2{\cdot}6H_2O$) and *N*,*N*-dimethylacetamide (DMAc) were purchased from Sinopharm Chemical Reagent Co. Ltd. All the other reagents were purchased from Aladdin Chemical Reagent Co. Ltd. and used as received without further purification. Deionized water was used throughout all the experiments.

2.2. Preparation of $Ni(OH)_2$/CNF hybrid membranes. As schematically illustrated in Figure 1, carbon nanofiber membranes

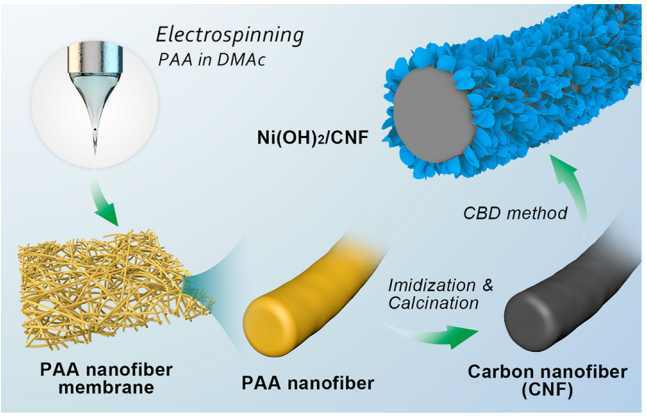

Figure 1. Schematic illustration of the preparation of flexible $Ni(OH)_2$/CNF hybrid membranes.

were prepared via the combination of electrospinning and subsequent carbonization. Poly(amic acid) (PAA) nanofiber membranes were obtained through a facile single-nozzle electrospinning technique. The PAA precursor for electrospinning was first synthesized by copolymerizing of PMDA and ODA in DMAc as described previously.[31] Then, the resulting viscous PAA solution was transferred into a 5 mL plastic syringe with a stainless steel needle. The electrospinning process was carreid out at an applied voltage of 20 kV with a feeding rate of 0.25 mm min^{-1} through the steel needle positioned 15 cm away from the aluminum drum collector. The generated PAA nanofiber membranes were thermally imidized under 300 °C and then carbonized at 1500 °C in a conventional tube furnace under N_2 atmosphere. After that, $Ni(OH)_2$/CNF hybrid membranes with different loading amounts of $Ni(OH)_2$ on carbon nanofibers were prepared by a CBD method. Typically, certain concentration of $Ni(NO_3)_2{\cdot}6H_2O$ (i.e., 0.01, 0.025 and 0.05 M, respectively) and 500 mg urea were dissolved into a mixed solution of 20 mL deionized water and 20 mL ethyl alcohol under stirring. Then the as-prepared CNF membranes were immersed in the above solution and heated to 70 °C in an oil bath for 4, 6, and 8 h, respectively. After cooling to room temperature, the obtained membranes were collected and rinsed with water for several times and dried at 50 °C under vacuum. For the control experiment, pure $Ni(OH)_2$ nanoplatelets were synthesized via the same method without the addition of CNF membranes.

2.3. Materials characterization. Morphology of the samples was investigated using field emission scanning electron microscope (FESEM, Ultra 55, Zeiss) at an acceleration voltage of 5 kV. Transmission electron microscopy (TEM) and high-resolution transmission electron microscopy (HRTEM) observations were performed with Tecnai G2 20 TWIN TEM under an acceleration

DOI: 10.1021/acsami.5b07528
ACS Appl. Mater. Interfaces 2015, 7, 22669−22677

voltage of 200 kV. All the TEM samples were first dispersed in aqueous solutions via sonication to form homogeneous suspensions. Then, the TEM samples were prepared by dropping the suspensions on the copper grids and drying in air. X-ray diffraction (XRD) patterns of the samples were conducted on an X'Pert Pro X-ray diffractometer with Cu K_α radiation (λ = 0.1542 nm) under a voltage of 40 kV and a current of 40 mA. X-ray photoelectron spectroscopy (XPS) analyses were carried out on a RBD upgraded PHI-5000C ESCA system (PerkinElmer) with Mg Kα radiation ($h\nu$ = 1253.6 eV) or Al Kα radiation ($h\nu$ = 1486.6 eV). All XPS spectra were corrected using C 1s line at 284.6 eV while curve fitting and background subtraction were accomplished using RBD AugerScan 3.21 software. Thermogravimetric analysis (TGA, Pyris 1) was performed under air flow from 100 to 800 °C at a heating rate of 10 °C min^{-1}. The Brunauer–Emmett–Teller (BET) surface area was measured using a Belsorp-max surface area detecting instrument by N_2 physisorption at 77 K. The electrical conductivity of the prepared samples was tested using a 4-Point Probes Resistivity Measurement System (RTS-8).

2.4. Electrochemical measurements. In order to evaluate the electrochemical performance, a three-electrode system was used, consisting of the sample modified glassy carbon electrode (GCE) as the working electrode, platinum as the counter electrode, and Ag/AgCl electrode as the reference electrode. The mass loading of a single supercapacitor electrode is 0.6–0.8 mg. The $Ni(OH)_2$/CNF hybrid membranes were fixed onto the glassy carbon electrode by using Nafion solution (Aladdin Chemical Reagent Co. Ltd.). Before the electrochemical tests, the as-prepared electrode was activated in a 2 M KOH aqueous electrolyte for 1 h. Cyclic voltammetry (CV) and galvanostatic charge/discharge tests, were carried out on a CHI 660D electrochemistry workstation (Shanghai Chenhua Instrument Co., China). Electrochemical impedance spectroscopy (EIS) was performed on a Princeton Applied Research PARSTAT 2273 instrument. CV curves were collected at different scan rates in a range from 0 to 0.6 V, and galvanostatic charge/discharge curves were measured in a voltage ranging from 0 to 0.4 V. The voltage window for CV test was extended so as to make sure that all the Faradaic redox reaction peaks of $Ni(OH)_2$/CNF electrodes were inside the collected voltage window. EIS was measured in the frequency range from 100 kHz to 0.01 Hz at open circuit potential with an AC voltage amplitude of 10 mV. The cycling tests for pure $Ni(OH)_2$ and $Ni(OH)_2$/CNF hybrid membranes were carried out by repeating the CV sweeps between 0 and 0.6 V at a scan rate of 20 mV s^{-1} for 1000 cycles. The specific capacitances were calculated from CV curves according to the following equation:

$$C = \int I \cdot dV / \upsilon \cdot m \cdot \Delta V \quad (1)$$

where I is the response current (A), V is the potential (V), υ is the scan rate (mV s^{-1}), and m is the mass of electroactive materials in the electrodes (g). The specific capacitances also can be calculated from galvanostatic charge/discharge curves according to the following equation:

$$C = \frac{I\Delta t}{m\Delta V} \quad (2)$$

where I is the charge or discharge current (A), Δt is the discharge time (s), m is the mass of electroactive materials in the electrodes (g), and ΔV is the potential window (V).

3. RESULTS AND DISCUSSION

3.1. Structure and morphology of $Ni(OH)_2$/CNF hybrid membranes. Electrospinning is a simple and efficient technique for fabricating self-standing nanofiber membranes with unique three-dimensional fiber network, good structural stability, and high flexibility. In this work, a free-standing CNF membrane is facilely obtained via electrospinning of PAA, and subsequent imidization and calcination processes. Figure 2 reveals that the electrospun carbon nanofibers have an average

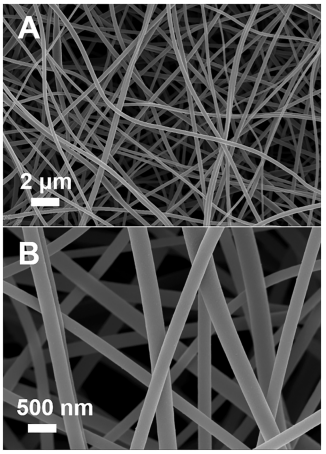

Figure 2. FESEM images of CNF membrane at (A) low and (B) high magnifications.

diameter of about 200–350 nm and a smooth surface without beads or breakages. Moreover, the nanofibers interconnected with each other are able to form a three-dimensional open architecture, which provides a high-surface-area template for further growth of electrochemically active materials to construct hierarchical nanocomposites. After that, a facile low-temperature chemical bath deposition process was utilized for in situ growth of crystallized $Ni(OH)_2$ nanoplatelets on carbon nanofibers. It can be clearly seen that the loading amount of $Ni(OH)_2$ nanoplatelets on carbon nanofibers obviously increases with increasing CBD time from 4 to 8 h at a fixed $Ni(NO_3)_2 \cdot 6H_2O$ concentration of 0.025 M (Figure 3). When the reaction time is 4 h, the carbon nanofibers are still not fully covered by $Ni(OH)_2$ nanoplatelets (Figure 3A and 3D). With further increasing reaction time to 6 h, thin $Ni(OH)_2$

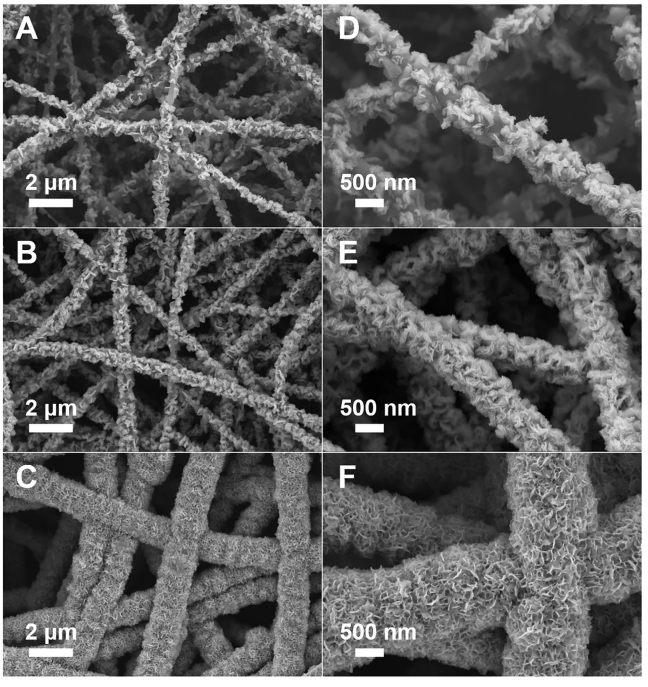

Figure 3. Low (left) and high (right) magnification FESEM images of $Ni(OH)_2$/CNF hybrid membranes prepared under different CBD reaction times: (A, D) 4 h; (B, E) 6 h; (C, F) 8 h.

DOI: 10.1021/acsami.5b07528
ACS Appl. Mater. Interfaces 2015, 7, 22669–22677

nanoplatelets with curled shape uniformly distribute throughout the surface of nanofibers (Figure 3B and 3E), which effectively prevents the aggregation of $Ni(OH)_2$ nanoplatelets and greatly increases the exposed active sites of $Ni(OH)_2$ nanoplatelets for rapid Faradaic reactions. However, after 8 h of reaction time, the deposition density of $Ni(OH)_2$ is sufficiently high that the $Ni(OH)_2$ nanoplatelets are densely accumulated and form a thick layer on the nanofibers (Figure 3C and 3F), which will definitely deteriorate the electron transport between $Ni(OH)_2$ nanoplatelets and the conductive carbon nanofibers, thus posing a negative effect on the capacitive performance of $Ni(OH)_2$/CNF hybrid membranes. In comparison, pure $Ni(OH)_2$ nanoplatelets prepared in the absence of CNF membranes severely aggregate into much larger spherical agglomerates (Figure S1, see ESI), implying the significance of the carbon nanofiber template for effectively dispersing $Ni(OH)_2$ nanoplatelets.

Furthermore, the effect of $Ni(NO_3)_2$ concentration on the growth of $Ni(OH)_2$ was studied at the fixed optimal CBD reaction time of 6 h. Here, the $Ni(OH)_2$/CNF hybrid membranes obtained from different concentrations of $Ni(NO_3)_2$ solution (0.01 M, 0.025 M, and 0.05 M) are denoted as $Ni(OH)_2$/CNF-0.01, $Ni(OH)_2$/CNF-0.025, and $Ni(OH)_2$/CNF-0.05, respectively. As displayed in Figure 4, the carbon

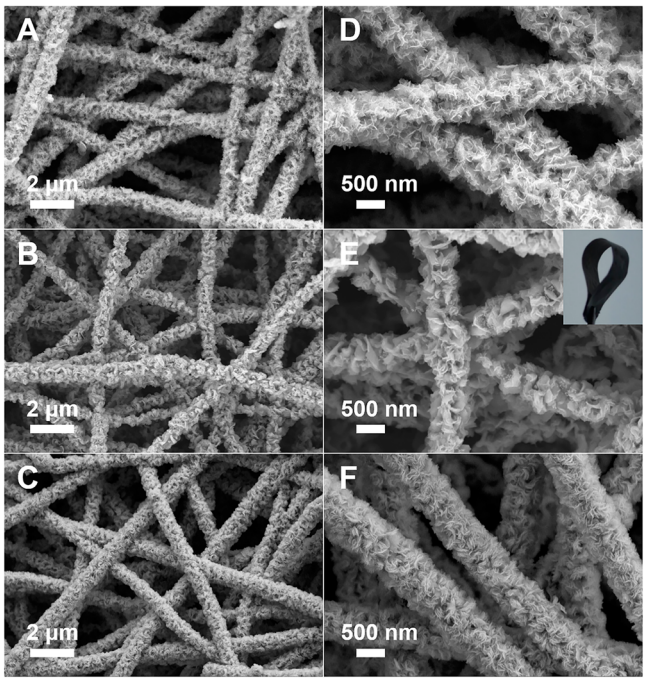

Figure 4. Low (left) and high (right) magnification FESEM images of $Ni(OH)_2$/CNF hybrid membranes obtained with different concentrations of $Ni(NO_3)_2$ solution: (A, D) 0.01 M; (B, E) 0.025 M; (C, F) 0.05 M. The inset of (E) shows the corresponding digital photo of the highly flexible $Ni(OH)_2$/CNF hybrid membrane.

nanofibers in all $Ni(OH)_2$/CNF hybrid membranes are fully covered by $Ni(OH)_2$ nanoplatelets. It can be seen that the density of $Ni(OH)_2$ nanoplatelets grown on the surface of carbon nanofibers increases and the size of $Ni(OH)_2$ nanoplatelets decreases with the increasing $Ni(NO_3)_2$ concentration. The carbon nanofibers are fully covered by relatively larger $Ni(OH)_2$ nanoplatelets in the $Ni(OH)_2$/CNF-0.01 hybrid membrane (Figure 4A and 4D). As for the $Ni(OH)_2$/CNF-0.025 hybrid membrane, smaller $Ni(OH)_2$ nanoplatelets begin to vertically grow on the surface of carbon nanofibers, forming hierarchical nanostructures (Figure 4B and 4E). The size of $Ni(OH)_2$ nanoplatelets becomes much smaller with further increasing $Ni(NO_3)_2$ concentration, but the deposition density of $Ni(OH)_2$ is sufficiently high that the $Ni(OH)_2$ nanoplatelets are densely accumulated on the carbon nanofibers in the $Ni(OH)_2$/CNF-0.05 hybrid membrane (Figure 4C and 4F), which will deteriorate the electron transfer between the $Ni(OH)_2$ sheath and carbon nanofiber core. Therefore, better interfacial interactions between the carbon nanofibers and $Ni(OH)_2$ nanoplatelets are achieved for the $Ni(OH)_2$/CNF-0.025 hybrid membrane. As displayed in Table S1 (see ESI), the electrical conductivities for CNF, $Ni(OH)_2$/CNF-0.01, $Ni(OH)_2$/CNF-0.025, and $Ni(OH)_2$/CNF-0.05 hybrid membranes are 1.62, 0.80, 1.05, and 0.56 S cm^{-1}, respectively. The $Ni(OH)_2$/CNF-0.025 hybrid membrane exhibits the best conductivity among all of the $Ni(OH)_2$/CNF hybrid membranes. The TEM image of the $Ni(OH)_2$/CNF-0.025 hybrid membrane (Figure 5A) reveals that $Ni(OH)_2$ nano-

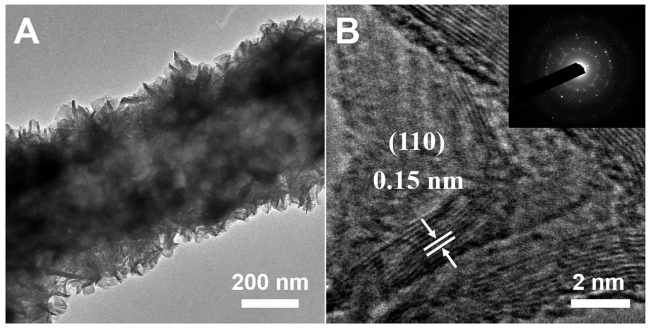

Figure 5. (A) TEM and (B) HRTEM images of the $Ni(OH)_2$/CNF-0.025 hybrid membrane. The inset of (B) is the corresponding SAED pattern of $Ni(OH)_2$ nanoplatelets grown on the carbon nanofibers.

platelets vertically and uniformly grow on the carbon nanofibers, which is in good agreement with the results from FESEM analysis. The HRTEM image of $Ni(OH)_2$ nanoplatelets (Figure 5B) exhibits the lattice fringe with lattice spacing of 0.15 nm, corresponding to the (110) plane of $Ni(OH)_2$. The corresponding SAED pattern (inset in Figure 5B) shows diffuse rings, indicating that the $Ni(OH)_2$ nanoplatelets are polycrystalline. Notably, 3D hierarchical nanostructures are nicely constructed with two-dimensional (2D) $Ni(OH)_2$ nanoplatelets homogeneously anchored on the one-dimensional (1D) carbon nanofibers, which can effectively prevent the aggregation of $Ni(OH)_2$ nanoplatelets and provide open and continuous channels for rapid diffusion of electrolyte to access the electrochemically active $Ni(OH)_2$ nanoplatelets. The BET analysis of nitrogen adsorption/desorption isotherms (Figure S2A, see ESI) strongly verifies the $Ni(OH)_2$/CNF-0.025 hybrid membrane as mesoporous materials with much larger specific surface area than the nonporous $Ni(OH)_2$ powder. As displayed in Figure S2B, the pore size distribution of the $Ni(OH)_2$/CNF-0.025 hybrid membrane calculated from the Barrett–Joiner–Halenda (BJH) method is mainly centered at 2–3 nm, which is in the mesoporous range. Moreover, it is worth mentioning that no crack is observed upon bending of the $Ni(OH)_2$/CNF-0.025 hybrid membrane (inset of Figure 4E). Notably, the $Ni(OH)_2$/CNF-0.025 hybrid membrane still remains highly flexible (Figure S3A) without breakage of the

DOI: 10.1021/acsami.5b07528
ACS Appl. Mater. Interfaces 2015, 7, 22669–22677

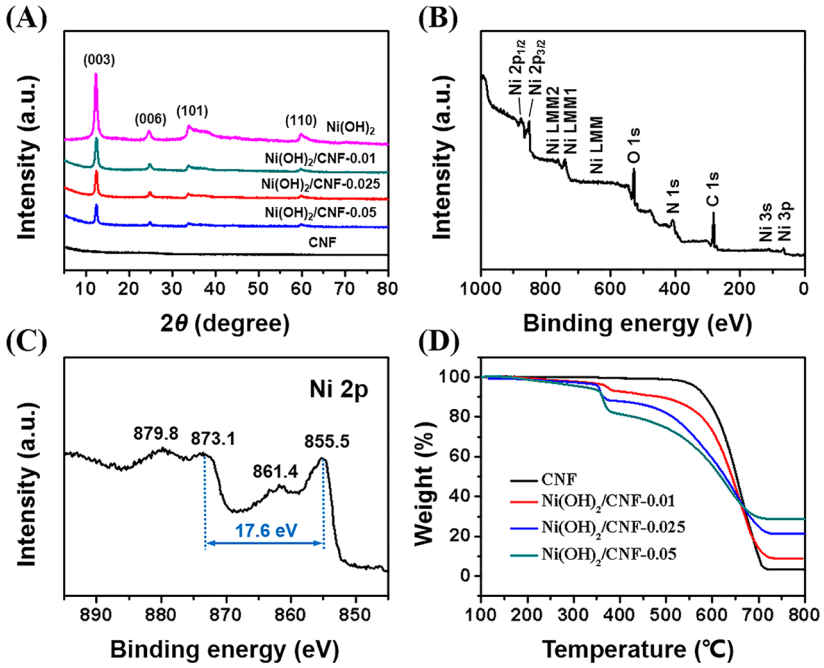

Figure 6. (A) XRD patterns of CNF membrane, pure $Ni(OH)_2$ powder, and $Ni(OH)_2$/CNF hybrid membranes. (B) XPS survey spectrum and (C) high-resolution Ni 2p spectrum of $Ni(OH)_2$/CNF-0.025 hybrid membrane. (D) TGA curves of CNF membrane and $Ni(OH)_2$/CNF hybrid membranes.

$Ni(OH)_2$/CNF nanofibers (Figure S3B) even after being bent back and forth 200 times, indicating its good flexibility and mechanical stability as a binder-free electrode for supercapacitors.

The crystal structures of pure $Ni(OH)_2$, CNF membranes, and $Ni(OH)_2$/CNF hybrid membranes were studied using XRD, as shown in Figure 6A. Both the pure $Ni(OH)_2$ powder and $Ni(OH)_2$/CNF hybrid membranes display four diffraction peaks at 2θ = 12.3°, 24.6°, 33.8°, and 59.8°, corresponding to the (003), (006), (101), and (110) planes of $Ni(OH)_2$ (JCPDS 38-0715), respectively, which indicate the formation of $Ni(OH)_2$ with good phase purity in the hybrid membranes.[32] Moreover, the difference between the intensity observed from the diffraction peaks of pure $Ni(OH)_2$ and $Ni(OH)_2$/CNF hybrid membranes is attributed to their different crystallite sizes and crystallinities.[33] The elemental compositions and chemical states of the $Ni(OH)_2$/CNF-0.025 hybrid membrane were further investigated by XPS analysis, with the survey spectrum revealing the coexistence of C, Ni, and O elements in the hybrid membrane (Figure 6B). The high-resolution spectrum of Ni 2p (Figure 6C) shows two main peaks at 855.5 and 873.1 eV (with a spin-energy separation of 17.6 eV), corresponding to Ni $2p_{3/2}$ and Ni $2p_{1/2}$, respectively. Furthermore, their associated satellite peaks located at 864.1 eV (Ni $2p_{3/2}$, satellite) and 879.8 eV (Ni $2p_{1/2}$, satellite) are also observed, which are typical characteristics of the $Ni(OH)_2$ phase and in good agreement with previous reports.[34]

The loading amounts of $Ni(OH)_2$ on the carbon nanofibers are determined by TGA analysis (Figure 6D). The TGA curves of $Ni(OH)_2$/CNF hybrid membranes exhibit two stages of thermal degradation, where the transformation of $Ni(OH)_2$ into NiO occurs at the first stage from 350 to 400 °C, while the second stage from 450 to 700 °C is related to the decomposition of CNFs. Since the pure CNF membrane is almost burned out at 800 °C, the loading amount of $Ni(OH)_2$ in the $Ni(OH)_2$/CNF hybrid membranes can be calculated from the residual fractions of the hybrid membranes,[35] which is 11.6, 25.5, and 31.7 wt % for $Ni(OH)_2$/CNF-0.01, $Ni(OH)_2$/CNF-0.025, and $Ni(OH)_2$/CNF-0.05 hybrid membranes, respectively. Notably, the pure CNF membrane shows excellent thermal stability with an onset degradation temperature over 500 °C. However, the decomposition temperature decreases after the incorporation of $Ni(OH)_2$, which is ascribed to the oxidative degradation of CNFs catalyzed by $Ni(OH)_2$. Nevertheless, the $Ni(OH)_2$/CNF hybrid membranes can still maintain excellent thermal stability with onset degradation temperatures over 400 °C.

3.2. Electrochemical performance of $Ni(OH)_2$/CNF hybrid membranes. To measure the electrochemical charge storage capacity, the CV curves of the CNF membrane, pure $Ni(OH)_2$ powder, $Ni(OH)_2$/CNF-0.01, $Ni(OH)_2$/CNF-0.025, and $Ni(OH)_2$/CNF-0.05 hybrid membranes are obtained (Figure 7). It can be seen that the CV curve of the CNF electrode exhibits a nearly rectangular shape due to the typical EDLC characteristic while the $Ni(OH)_2$/CNF electrodes show a couple of redox peaks in the potential range from 0 to 0.6 V,

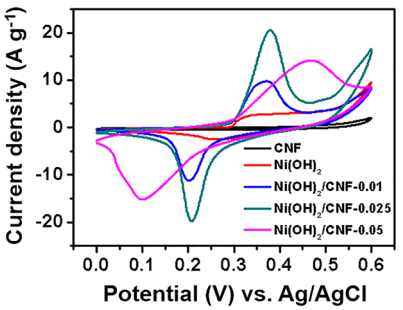

Figure 7. CV curves of CNF membrane, pure $Ni(OH)_2$ powder, $Ni(OH)_2$/CNF-0.01, $Ni(OH)_2$/CNF-0.025, and $Ni(OH)_2$/CNF-0.05 hybrid membranes at a scan rate of 20 mV s^{-1}.

DOI: 10.1021/acsami.5b07528
ACS Appl. Mater. Interfaces 2015, 7, 22669−22677

indicating that the energy storage mechanism of $Ni(OH)_2$/CNF hybrid membranes is mainly associated with Faradaic redox reactions between $Ni(OH)_2$ and NiOOH in alkaline solution as follows:[36,37]

$$Ni(OH)_2 + OH^- \leftrightarrow NiOOH + H_2O + e^- \quad (3)$$

Moreover, $Ni(OH)_2$/CNF hybrid membranes display much higher current density and larger CV areas than those of CNFs and pure $Ni(OH)_2$, which reveals the greatly improved electrochemical performances of the hybrid membranes compared to their individual counterparts. The remarkably improved capacitance of $Ni(OH)_2$/CNF hybrid membranes can be ascribed to the synergistic effects between 1D carbon nanofibers and 2D $Ni(OH)_2$ nanoplatelets, where thin $Ni(OH)_2$ nanoplatelets are vertically and uniformly anchored on the carbon nanofibers instead of forming aggregations, thus providing higher specific surface area and more exposure of active sites for efficient electrochemical interactions with the electrolyte compared to pure $Ni(OH)_2$ powder (Figure 8).

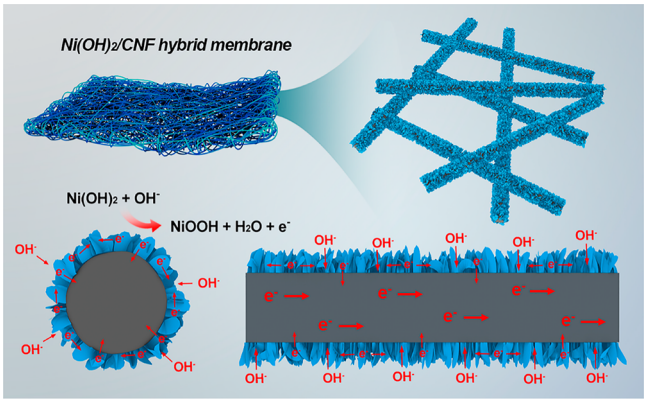

Figure 8. Schematic illustration of the ion diffusion and electron transportation in $Ni(OH)_2$/CNF hybrid membrane.

Additionally, the overall 3D macroporous architectures as well as the hierarchical nanostructures of $Ni(OH)_2$/CNF hybrid membranes can significantly shorten the ion diffusion length, enhance the contact area, and ensure ion/electron diffusion with low resistance. Moreover, the highly conductive carbon nanofibers can act as the conductive core to provide efficient electron transport for fast Faradaic redox reactions of the electrochemically active $Ni(OH)_2$ sheath, leading to greatly improved electrochemical performance.

The rate capabilities of $Ni(OH)_2$/CNF hybrid membranes at various scan rates are presented in Figure 9A–9C. As for $Ni(OH)_2$/CNF-0.1 and $Ni(OH)_2$/CNF-0.025 hybrid membranes, the shape of CV curves has no obvious change with the increasing scan rates despite the enhancement of current densities (Figure 9A and 9B), suggesting their superior rate stability. However, the shape of CV curves for the $Ni(OH)_2$/CNF-0.05 hybrid membrane becomes disordered and the redox peaks disappear as the scan rate increases (Figure 9C). The inferior rate stability may originate from the excessively thick coating layer of $Ni(OH)_2$ nanoplatelets on carbon nanofibers, which will severely decrease the exposure of electrochemically active sites and fail to afford the fast redox reactions at high scan rates. Additionally, the anodic and cathodic peaks in the CV curves of $Ni(OH)_2$/CNF electrodes shift positively and negatively with the increasing scan rates, respectively, corresponding to the serious electric polarization during the faradaic redox processes at high scan rates.[38,39] Calculated from the above CV curves, the specific capacitances of $Ni(OH)_2$/CNF-0.01, $Ni(OH)_2$/CNF-0.025, and $Ni(OH)_2$/CNF-0.05 hybrid membranes are determined to be 2496 F g^{-1}, 2523 F g^{-1}, and 2428 F g^{-1}, respectively (based on the mass of $Ni(OH)_2$, at a scan rate of 5 mV s^{-1}), that is 357 F g^{-1}, 701 F g^{-1}, and 822 F g^{-1} (based on the total mass, at a scan rate of 5 mV s^{-1}). The specific capacitance retention of $Ni(OH)_2$/CNF-0.01, $Ni(OH)_2$/CNF-0.025, and $Ni(OH)_2$/CNF-0.05 hybrid membranes is 61%, 68%, and 17% at a scan rate of 100 mV s^{-1}, respectively. In comparison with the graphene/$Ni(OH)_2$ and $Ni(OH)_2$/carbon nanotubes/Ni foam electrode materials reported previously,[32,40] $Ni(OH)_2$/CNF hybrid membranes show comparable capacitive performance with a much easier preparation process.

Figure 9D–9F demonstrate galvanostatic charge–discharge curves of CNF membrane, pure $Ni(OH)_2$ powder, and $Ni(OH)_2$/CNF-0.025 hybrid membrane at various current densities. The curves of CNF membrane show well-defined isosceles triangle shapes (Figure 9D), indicating its typical EDLC characteristic, whereas the charge–discharge curves of $Ni(OH)_2$/CNF hybrid membranes and pure $Ni(OH)_2$ exhibit a general pseudocapacitive behavior (Figure 9E and 9F). The $Ni(OH)_2$/CNF-0.025 hybrid membrane delivers a high capacitance of 2394 F g^{-1} at 1 A g^{-1} based on the mass of $Ni(OH)_2$ (that is 667 F g^{-1} based on the total mass) according to the charge–discharge curves, while the specific capacitance of pure $Ni(OH)_2$ is only 235 F g^{-1} at a current density of 1 A g^{-1}. The results are in good accordance with those calculated from CV curves. The remarkably enhanced capacitance of $Ni(OH)_2$/CNF hybrid membranes is attributed to their overall 3D macroporous architectures derived from the electrospun CNF networks, which can greatly increase the porosity and facilitate the rapid diffusion of ions to access the $Ni(OH)_2$ nanoplatelets. Moreover, the hierarchical nanostructures with $Ni(OH)_2$ nanoplatelets homogeneously anchored on the carbon nanofibers can ensure better electrical contact and interfacial interactions between the $Ni(OH)_2$ sheath and conductive carbon nanofiber core, thus providing efficient transport of electrons across the interfaces for fast Faradaic redox reactions and leading to greatly enhanced capacitive performance.

Not only high specific capacitance but also good long-term stability is desirable for promising electrode materials in supercapacitors.[41,42] The cycling tests for $Ni(OH)_2$/CNF-0.025 hybrid membranes and pure $Ni(OH)_2$ powder were conducted by sweeping the CV curves from 0 to 0.6 V at a scan rate of 20 mV s^{-1} for 1000 cycles. As exhibited in Figure 10, the specific capacitance of $Ni(OH)_2$/CNF-0.025 hybrid membranes increases by about 10% during the first 200 cycles due to the activation effect that allows the trapped ions gradually diffuse outward. Besides, the $Ni(OH)_2$/CNF-0.025 hybrid membrane shows about 83% retention after 1000 cycles, which is much higher than the 47% retention for pure $Ni(OH)_2$. The remarkably improved electrochemical stability of $Ni(OH)_2$/CNF-0.025 hybrid membrane can be explained as follows. In the hybrid membrane, the carbon nanofiber can act both as a buffering matrix to accommodate the local volumetric expansion/contraction of $Ni(OH)_2$ nanoplatelets upon long-term cycling, and as a conductive core to provide efficient transport of electrons for stable Faradaic redox reactions of the $Ni(OH)_2$ sheath. Thus, the morphological and electrochemical changes of $Ni(OH)_2$ nanoplatelets induced by charge/discharge

DOI: 10.1021/acsami.5b07528
ACS Appl. Mater. Interfaces 2015, 7, 22669–22677

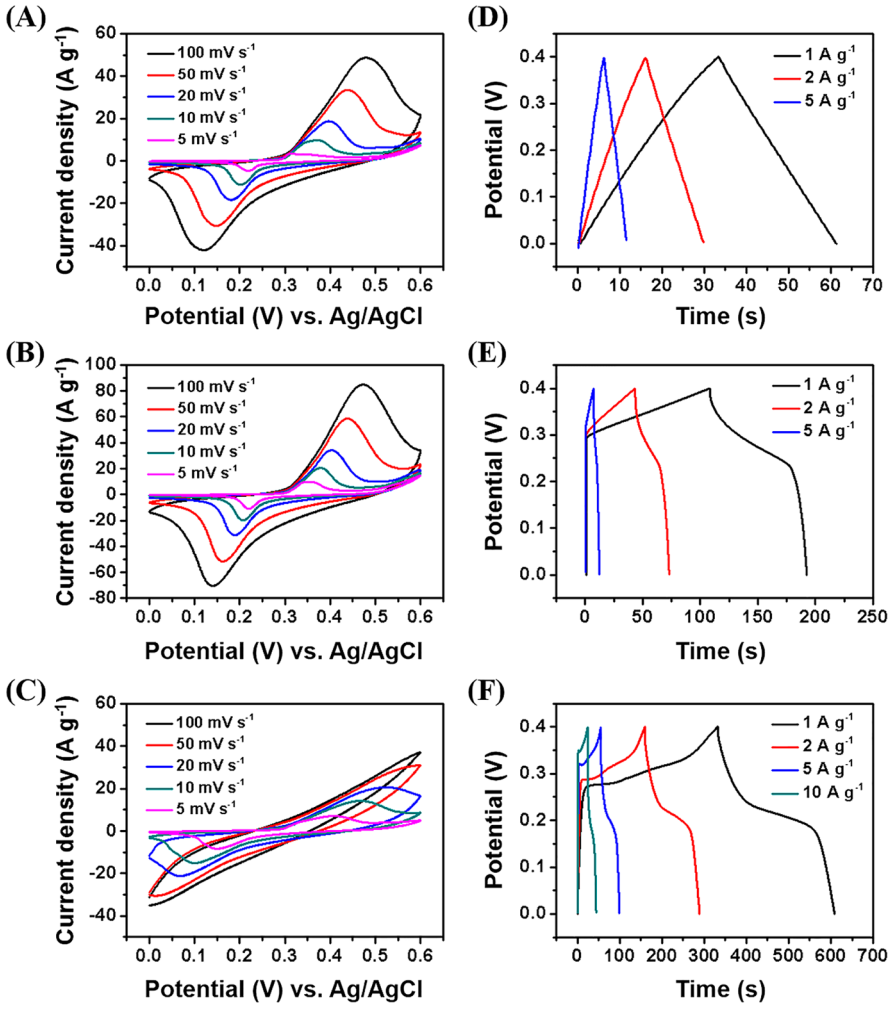

Figure 9. CV curves of (A) $Ni(OH)_2$/CNF-0.01, (B) $Ni(OH)_2$/CNF-0.025, and (C) $Ni(OH)_2$/CNF-0.05 hybrid membranes at different scan rates. Galvanostatic charge–discharge curves of (D) CNF membrane, (E) pure $Ni(OH)_2$, and (F) $Ni(OH)_2$/CNF-0.025 hybrid membrane at different current densities.

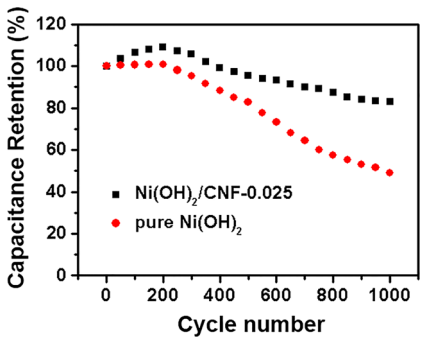

Figure 10. Cycling performance of pure $Ni(OH)_2$ powder and $Ni(OH)_2$/CNF-0.025 hybrid membrane at a scan rate of 20 mV s^{-1} for 1000 cycles.

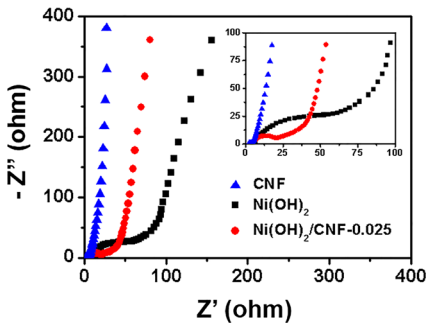

Figure 11. Nyquist plots of CNF membrane, pure $Ni(OH)_2$ powder, and $Ni(OH)_2$/CNF-0.025 hybrid membrane measured in the frequency range from 100 kHz to 0.01 Hz with an AC voltage amplitude of 10 mV.

cycling are greatly reduced, ensuring a remarkably enhanced cycling performance of the $Ni(OH)_2$/CNF hybrid membranes.

To better understand the superior electrochemical performance of $Ni(OH)_2$/CNF hybrid membranes, EIS analysis was carried out to investigate the AC impedance of the CNF membrane, pure $Ni(OH)_2$ powder, and $Ni(OH)_2$/CNF-0.025 hybrid membrane (Figure 11). Generally, the Nyquist plot consists of a semicircle in the high-frequency region and a straight line in the low-frequency region, corresponding to the charge transfer resistance and ion diffusion resistance in the electrode, respectively.[43] The slope of the 45° portion of the curve between the high-frequency region and the low-frequency region is called the Warburg resistance, which is a result of the frequency dependence of ion diffusion in the electrolyte to the electrode interface.[44] As shown in Figure 11, the Nyquist plots of both $Ni(OH)_2$ and $Ni(OH)_2$/CNF-0.025 electrodes show a

DOI: 10.1021/acsami.5b07528
ACS Appl. Mater. Interfaces 2015, 7, 22669–22677

single semicircle in the high-frequency region and a straight line in the low-frequency region, which are related to the charge transfer processes and the ion diffusion processes, respectively. The $Ni(OH)_2$/CNF-0.025 electrode displays a much smaller radius of semicircle in the high-frequency region compared to that of the $Ni(OH)_2$ electrode, indicating its lower faradaic charge transfer resistance. Besides, the $Ni(OH)_2$/CNF-0.025 electrode exhibits a more vertical line than the $Ni(OH)_2$ electrode in the low-frequency region, illustrating better capacitive behavior and lower diffusion resistance of ions. It is worth mentioning that the Nyquist plot of the CNF electrode does not exhibit a semicircle in the high-frequency region, due to its low charge transfer resistance. The straight line of the CNF electrode in the low-frequency region is more vertical than those of the $Ni(OH)_2$/CNF-0.025 and $Ni(OH)_2$ electrodes, demonstrating the best conductivity among these three electrodes. These results confirm that the carbon nanofiber matrix can significantly enhance the electrical conductivity of the $Ni(OH)_2$/CNF-0.025 hybrid membrane, thus leading to significant improvement of the electrochemical performance.

4. CONCLUSIONS

In summary, highly flexible $Ni(OH)_2$/CNF hybrid membranes with ultrathin $Ni(OH)_2$ nanoplatelets vertically and uniformly anchored on the carbon nanofibers have been facilely prepared as supercapacitor electrode materials through the combination of electrospinning and chemical bath deposition. The carbon nanofibers with excellent electrical conductivity and structural stability not only facilitate the charge transfer across the interfaces for fast Faradaic redox reactions of $Ni(OH)_2$ nanoplatelets but also effectively mitigate their aggregation and volumetric expansion upon long-term cycling. Moreover, the overall 3D macroporous architectures as well as the hierarchical nanostructures of $Ni(OH)_2$/CNF hybrid membranes can provide open and continuous channels, which enable rapid diffusion of electrolyte to access the electrochemically active $Ni(OH)_2$ nanoplatelets. Benefiting from the synergistic effects, the optimized $Ni(OH)_2$/CNF hybrid membrane exhibits a high specific capacitance of 2523 F g^{-1} based on the mass of $Ni(OH)_2$ (that is 701 F g^{-1} based on the total mass) at a scan rate of 5 mV s^{-1} and a long cycle life of 83% capacitance retention after 1000 cycles, making it a promising candidate as flexible electrode material for applications in high-performance supercapacitors.

■ ASSOCIATED CONTENT

Supporting Information

The Supporting Information is available free of charge on the ACS Publications website at DOI: 10.1021/acsami.5b07528.

FESEM images of pure $Ni(OH)_2$; nitrogen adsorption/desorption isotherms of pure $Ni(OH)_2$ powder and the $Ni(OH)_2$/CNF-0.025 hybrid membrane; the corresponding pore size distribution of the $Ni(OH)_2$/CNF-0.025 hybrid membrane; digital photo and FESEM image of the $Ni(OH)_2$/CNF-0.025 hybrid membrane after being repeatedly bent back and forth 200 times (PDF)

■ AUTHOR INFORMATION

Corresponding Authors

*(Y. E. Miao) E-mail: 12110440023@fudan.edu.cn.

*(T. X. Liu) E-mail: txliu@fudan.edu.cn; Tel: +86-21-55664197; Fax: +86-21-65640293.

Notes

The authors declare no competing financial interest.

■ ACKNOWLEDGMENTS

The authors are grateful for the financial support from the National Natural Science Foundation of China (51125011, 51373037, 51433001).

■ REFERENCES

(1) Lai, C. H.; Lu, M. Y.; Chen, L. J. Metal Sulfide Nanostructures: Synthesis, Properties and Applications in Energy Conversion and Storage. *J. Mater. Chem.* **2012**, *22*, 19−30.

(2) Manthiram, A.; Vadivel Murugan, A.; Sarkar, A.; Muraliganth, T. Nanostructured Electrode Materials for Electrochemical Energy Etorage and Conversion. *Energy Environ. Sci.* **2008**, *1*, 621−638.

(3) Arico, A. S.; Bruce, P.; Scrosati, B.; Tarascon, J.; van Schalkwijk, W. Nanostructured Materials for Advanced Energy Conversion and Storage Devices. *Nat. Mater.* **2005**, *4*, 366−377.

(4) Barber, J. Photosynthetic Energy Conversion: Natural and Artificial. *Chem. Soc. Rev.* **2009**, *38*, 185−196.

(5) Lewis, N. S. Toward Cost-Effective Solar Energy Use. *Science* **2007**, *315*, 798−801.

(6) Wang, H. L.; Liang, Y. Y.; Mirfakhrai, T.; Chen, Z.; Casalongue, H.; Dai, H. J. Advanced Asymmetrical Supercapacitors Based on Graphene Hybrid Materials. *Nano Res.* **2011**, *4*, 729−736.

(7) Pumera, M. Graphene-Based Nanomaterials for Energy Storage. *Energy Environ. Sci.* **2011**, *4*, 668−674.

(8) Chen, S.; Duan, J. J.; Jaroniec, M.; Qiao, S. Z. Hierarchically Porous Graphene-Based Hybrid Electrodes with Excellent Electrochemical Performance. *J. Mater. Chem. A* **2013**, *1*, 9409−9413.

(9) Yang, N. L.; Zhai, J.; Wang, D.; Chen, Y. S.; Jiang, L. Two-Dimensional Graphene Bridges Enhanced Photoinduced Charge Transport in Dye-Sensitized Solar Cells. *ACS Nano* **2010**, *4*, 887−894.

(10) Feng, J. X.; Ye, S. H.; Lu, X. F.; Tong, Y. X.; Li, G. R. Asymmetric Paper Supercapacitor Based on Amorphous Porous Mn_3O_4 Negative Electrode and $Ni(OH)_2$ Positive Electrode: A Novel and High-Performance Flexible Electrochemical Energy Storage Device. *ACS Appl. Mater. Interfaces* **2015**, *7*, 11444−11451.

(11) Frackowiak, E. Carbon Materials for Supercapacitor Application. *Phys. Chem. Chem. Phys.* **2007**, *9*, 1774−1785.

(12) Frackowiak, E.; Béguin, F. Carbon Materials for the Electrochemical Storage of Energy in Capacitors. *Carbon* **2001**, *39*, 937−950.

(13) Zhang, L. L.; Zhao, X. S. Carbon-Based Materials as Supercapacitor Electrodes. *Chem. Soc. Rev.* **2009**, *38*, 2520−2531.

(14) Zhang, Y.; Feng, H.; Wu, X. B.; Wang, L. Z.; Zhang, A. Q.; Xia, T. C.; Dong, H. C.; Li, X. F.; Zhang, L. S. Progress of Electrochemical Capacitor Electrode Materials: A Review. *Int. J. Hydrogen Energy* **2009**, *34*, 4889−4899.

(15) Kuo, S.; Wu, N. Investigation of Pseudocapacitive Charge-Storage Reaction of $MnO_2{\cdot}nH_2O$ Supercapacitors in Aqueous Electrolytes. *J. Electrochem. Soc.* **2006**, *153*, 1317−1324.

(16) Khomenko, V.; Raymundo-Piñero, E.; Béguin, F. Optimisation of An Asymmetric Manganese Oxide/Activated Carbon Capacitor Working at 2 V in Aqueous Medium. *J. Power Sources* **2006**, *153*, 183−190.

(17) Banerjee, P. C.; Lobo, D. E.; Middag, R.; Ng, W. K.; Shaibani, M. E.; Majumder, M. Electrochemical Capacitance of Ni-Doped Metal Organic Framework and Reduced Graphene Oxide Composites: More Than the Sum of Its Parts. *ACS Appl. Mater. Interfaces* **2015**, *7*, 3655−3664.

(18) Fan, Z. J.; Yan, J.; Wei, T.; Zhi, L. J.; Ning, G. Q.; Li, T. Y.; Wei, F. Asymmetric Supercapacitors Based on Graphene/MnO_2 and Activated Carbon Nanofiber Electrodes with High Power and Energy Density. *Adv. Funct. Mater.* **2011**, *21*, 2366−2375.

(19) Kong, D. S.; Wang, J. M.; Shao, H. B.; Zhang, J. Q.; Cao, C. N. Electrochemical Fabrication of A Porous Nanostructured Nickel Hydroxide Film Electrode with Superior Pseudocapacitive Performance. *J. Alloys Compd.* **2011**, *509*, 5611−5616.

DOI: 10.1021/acsami.5b07528
ACS Appl. Mater. Interfaces 2015, 7, 22669−22677

(20) Chen, Z.; Augustyn, V.; Wen, J.; Zhang, Y. W.; Shen, M. Q.; Dunn, B.; Lu, Y. F. High-Performance Supercapacitors Based on Intertwined CNT/V_2O_5 Nanowire Nanocomposites. *Adv. Mater.* **2011**, *23*, 791−795.
(21) Li, J. T.; Zhao, W.; Huang, F. Q.; Manivannan, A.; Wu, N. Q. Single-Crystalline $Ni(OH)_2$ and NiO Nanoplatelet Arrays as Supercapacitor Electrodes. *Nanoscale* **2011**, *3*, 5103−5109.
(22) Cai, J.; Niu, H. T.; Li, Z. Y.; Du, Y.; Cizek, P.; Xie, Z. L.; Xiong, H. G.; Lin, T. High-Performance Supercapacitor Electrode Materials from Cellulose-Derived Carbon Nanofibers. *ACS Appl. Mater. Interfaces* **2015**, *7*, 14946−14953.
(23) Wang, R. T.; Lang, J. W.; Liu, Y. H.; Lin, Z. Y.; Yan, X. B. Ultra-Small, Size-Controlled $Ni(OH)_2$ Nanoparticles: Elucidating the Relationship between Particle Size and Electrochemical Performance for Advanced Energy Storage Devices. *NPG Asia Mater.* **2015**, *7*, 183.
(24) Ma, X. W.; Li, Y.; Wen, Z. W.; Gao, F. X.; Liang, C. Y.; Che, R. C. Ultrathin beta-$Ni(OH)_2$ Nanoplates Vertically Grown on Nickel-Coated Carbon Nanotubes as High-Performance Pseudocapacitor Electrode Materials. *ACS Appl. Mater. Interfaces* **2015**, *7*, 974−979.
(25) Hosogai, S.; Tsutsumi, H. Electrospun Nickel Oxide/Polymer Fibrous Electrodes for Electrochemical Capacitors and Effect of Heat Treatment Process on Their Performance. *J. Power Sources* **2009**, *194*, 1213−1217.
(26) Zhi, M. J.; Manivannan, A.; Meng, F. K.; Wu, N. Q. Highly Conductive Electrospun Carbon Nanofiber/MnO_2 Coaxial Nano-Cables for High Energy and Power Density Supercapacitors. *J. Power Sources* **2012**, *208*, 345−353.
(27) Zhou, G.; Zhu, J.; Chen, Y. J.; Mei, L.; Duan, X. C.; Zhang, G. H.; Chen, L. B.; Wang, T. H.; Lu, B. A. Simple Method for the Preparation of Highly Porous $ZnCo_2O_4$ Nanotubes with Enhanced Electrochemical Property for Supercapacitor. *Electrochim. Acta* **2014**, *123*, 450−455.
(28) Wang, Q. J.; Song, W. L.; Wang, L. N.; Song, Y.; Shi, Q.; Fan, L. Z. Electrospun Polyimide-Based Fiber Membranes as Polymer Electrolytes for Lithium-Ion Batteries. *Electrochim. Acta* **2014**, *132*, 538−544.
(29) Cheng, C. Y.; Chen, J.; Chen, F.; Hu, P.; Wu, X. F.; Reneker, D. H.; Hou, H. Q. High-Strength and High-Toughness Polyimide Nanofibers: Synthesis and Characterization. *J. Appl. Polym. Sci.* **2010**, *116*, 1581−1586.
(30) Xuyen, N. T.; Ra, E. J.; Geng, H. Z.; Kim, K. K.; An, K. H.; Lee, Y. H. Enhancement of Conductivity by Diameter Control of Polyimide-Based Electrospun Carbon Nanofibers. *J. Phys. Chem. B* **2007**, *111*, 11350−11353.
(31) Ding, Q. W.; Miao, Y. E.; Liu, T. X. Morphology and Photocatalytic Property of Hierarchical Polyimide/ZnO Fibers Prepared via A Direct Ion-Exchange Process. *ACS Appl. Mater. Interfaces* **2013**, *5*, 5617−5622.
(32) Yang, S. B.; Wu, X. L.; Chen, C. L.; Dong, H. L.; Hu, W. P.; Wang, X. K. Spherical alpha-$Ni(OH)_2$ Nanoarchitecture Grown on Graphene as Advanced Electrochemical Pseudocapacitor Materials. *Chem. Commun.* **2012**, *48*, 2773−2775.
(33) Zhang, H. T.; Zhang, X.; Zhang, D. C.; Sun, X. Z.; Lin, H.; Wang, C. H.; Ma, Y. W. One-Step Electrophoretic Deposition of Reduced Graphene Oxide and $Ni(OH)_2$ Composite Films for Controlled Syntheses Supercapacitor Electrodes. *J. Phys. Chem. B* **2013**, *117*, 1616−1627.
(34) Chen, H.; Zhou, S. X.; Wu, L. M. Porous Nickel Hydroxide Manganese Dioxide-Reduced Graphene Oxide Ternary Hybrid Spheres as Excellent Supercapacitor Electrode Materials. *ACS Appl. Mater. Interfaces* **2014**, *6*, 8621−8630.
(35) Al-Enizi, A. M.; Elzatahry, A. A.; Abdullah, A. M.; AlMaadeed, M. A.; Wang, J. X.; Zhao, D. Y.; Al-Deyab, S. Synthesis and Electrochemical Properties of Nickel Oxide/Carbon Nanofiber Composites. *Carbon* **2014**, *71*, 276−283.
(36) Jiang, L.; Zou, R. J.; Li, W. Y.; Sun, J. Q.; Hu, X. H.; Xue, Y. F.; He, G. J.; Hu, J. Q. $Ni(OH)_2$/CoO/Reduced Graphene Oxide Composites with Excellent Electrochemical Properties. *J. Mater. Chem. A* **2013**, *1*, 478−481.
(37) Yang, D. G.; Wang, F.; Yan, J.; Gao, Y.; Li, H. M. Preparation, Characterization, and Electrochemical Performances of Graphene/$Ni(OH)_2$ Hybrid Nanomaterials. *J. Nanopart. Res.* **2013**, *15*, 1−14.
(38) Yan, J.; Fan, Z. J.; Sun, W.; Ning, G. Q.; Wei, T.; Zhang, Q.; Zhang, R. F.; Zhi, L. J.; Wei, F. Advanced Asymmetric Supercapacitors Based on $Ni(OH)_2$/Graphene and Porous Graphene Electrodes with High Energy Density. *Adv. Funct. Mater.* **2012**, *22*, 2632−2641.
(39) Yin, H. Y.; Wang, D. H.; Zhu, H.; Xiao, W.; Gan, F. X. Growing Highly Capacitive Nano-$Ni(OH)_2$ on Freshly Cut Graphite Electrode by Electrochemically Enhanced Self-assembly. *Electrochim. Acta* **2013**, *99*, 198−203.
(40) Tang, Z.; Tang, C. H.; Gong, H. A High Energy Density Asymmetric Supercapacitor from Nano-Architectured $Ni(OH)_2$/Carbon Nanotube Electrodes. *Adv. Funct. Mater.* **2012**, *22*, 1272−1278.
(41) Wu, Z.; Huang, X. L.; Wang, Z. L.; Xu, J. J.; Wang, H. G.; Zhang, X. B. Electrostatic Induced Stretch Growth of Homogeneous β-$Ni(OH)_2$ on Graphene with Enhanced High-Rate Cycling for Supercapacitors. *Sci. Rep.* **2014**, *4*, 3699.
(42) Wang, X.; Wang, Y. Y.; Zhao, C. M.; Zhao, Y. X.; Yan, B. Y.; Zheng, W. T. Electrodeposited $Ni(OH)_2$ Nanoflakes on Graphite Nanosheets Prepared by Plasma-Enhanced Chemical Vapor Deposition for Supercapacitor Electrode. *New J. Chem.* **2012**, *36*, 1902−1906.
(43) Li, J.; Xie, H. Q.; Li, Y.; Liu, J.; Li, Z. X. Electrochemical Properties of Graphene Nanosheets/Polyaniline Nanofibers Composites as Electrode for Supercapacitors. *J. Power Sources* **2011**, *196*, 10775−10781.
(44) Wang, Y.; Shi, Z. Q.; Huang, Y.; Ma, Y. F.; Wang, C. Y.; Chen, M. M.; Chen, Y. S. Supercapacitor Devices Based on Graphene Materials. *J. Phys. Chem. C* **2009**, *113*, 13103−13107.

DOI: 10.1021/acsami.5b07528
ACS Appl. Mater. Interfaces 2015, 7, 22669−22677